# Evaluating Donor Effects in Isoindigo Based Small

# Molecular Fluorophores

Sajith M. Vijayan, <sup>1</sup> Nicholas Sparks, <sup>1</sup> Juganta K. Roy, <sup>2</sup> Cameron Smith, <sup>1</sup> Christopher Tate, <sup>1</sup> Nathan I. Hammer, <sup>1</sup> Jerzy Leszczynski<sup>2\*</sup> and Davita L. Watkins <sup>1\*</sup>

<sup>1</sup>Department of Chemistry and Biochemistry, University of Mississippi, Oxford, MS 38677, United States

<sup>2</sup>Interdisciplinary Center for Nanotoxicity, Department of Chemistry, Physics and Atmospheric Sciences, Jackson State University, Jackson, MS 39217, United States

ABSTRACT: Small molecular organic fluorophores have garnered significant interest because of their indispensable use in fluorescence imaging (FI) and optoelectronic devices. Herein, we designed triphenylamine (TPA) capped donor-acceptor-donor (D-A-D) based fluorophores having a variation at the heterocyclic donor (D) units, 3,4-ethylenedioxythiophene (EDOT), furan (FURAN), thiophene (THIO), and 1-methyl-1H-pyrrole (MePyr), with isoindigo as the core electron acceptor (A) unit. Synthesis of these fluorophores (II-X-TPA) resulted in four symmetrical dye molecules: II-EDOT-TPA, II-FURAN-TPA, II-THIO-TPA, and II-MePyr-TPA where TPA functioned as a terminal unit as well as a secondary electron donor group. Photophysical, electrochemical, and computational analysis was conducted to investigate the effect of heterocyclic donor units on the II-X-TPA derivatives. Density functional theory (DFT)

and time-dependent DFT (TD-DFT) calculations provided insightful features of structural and the electronic properties of each fluorophore and correlated well with experimental observations. Electron density distribution maps, overlapping frontier molecular orbitals (FMOs) diagrams and highest occupied molecular orbital (HOMO) to lowest unoccupied molecular orbital (LUMO) electron transfer indicated intramolecular charge transfer (ICT). Theoretical studies confirmed the experimental HOMO energies trend and demonstrated their crucial importance in understanding each heterocycles donor ability. Stokes shifts of up to ~178 nm were observed whereas, absorptions and emissions were shifted deeper into the NIR region resulting from ICT. Results suggest that this isoindigo fluorophore series has potential as a molecular scaffold for the development of efficient FI agents. Studied fluorophores can be further tuned with different donor fragments to enhance the ICT and facilitate in shifting the optical properties further into the NIR region.

## **INTRODUCTION**

Fluorescence imaging (FI) has received momentous attention over the last decade as a noninvasive approach to monitor physiological diseases associated with human organs, guide surgical interventions and evaluate treatment efficacy. 1–4 FI using small organic fluorophores has been widely studied due to their potential advantages that include well-defined structural design, tunable optical properties, and lowered toxicity compared to traditional tomographic imaging techniques. 5–8 There are only a few small molecular organic fluorophores that have been FDA approved for in vivo imaging such as ICG (indocyanine green,  $\lambda_{max}^{abs} = 807$  nm and  $\lambda_{max}^{ems} = 822$  nm) and MB (methylene blue,  $\lambda_{max}^{abs} = 665$  nm and  $\lambda_{max}^{ems} = 686$  nm). 12,13 They are excellent NIR dyes that have high molar absorptivity, strong fluorescence, and good photostability. However, their

intrinsically small Stokes shifts lead to self-quenching and fluorescence detection error that results in poor image quality.14–16 One approach to address this issue is to develop a small molecular fluorophore with a large Stokes shift which improves the signal to noise ratio of the fluorescence image by reducing the overlap between the UV absorption and emission spectrum.17–20 This improvement will minimize the back absorption of the emitted photons, providing more photons to produce the image.

Herein, we synthesized a series of small molecular dye fluorophores with large Stokes shift using the widely applied donor-acceptor-donor (D-A-D) architecture. We explore donor engineering to develop high-performance small molecule fluorophores and investigate the relationship between the donor structures and fluorescence properties. In the design of NIR-emitting fluorophores, the energy gap between the highest occupied molecular orbital (HOMO) and the lowest unoccupied molecular orbital (LUMO) is known to be significantly affected by conjugation length as well as donor-acceptor (D-A) charge transfer within a  $\pi$ -conjugated framework.21,22 Adding an extra donor and forming a D-A-D architecture is the key to achieving an organic fluorophore with longer emission wavelength by further reducing the energy gap.23–25 Alternatively, emission wavelengths can be improved via heteroatom substitutions and the introduction of polymethine molecules.26,27 However, having a large conjugated backbone induces fluorescence quenching by intensifying intermolecular interactions.28,29 Such considerations are beneficial for the development of simple molecular fluorophores that can be further modified to enhance their efficiency.

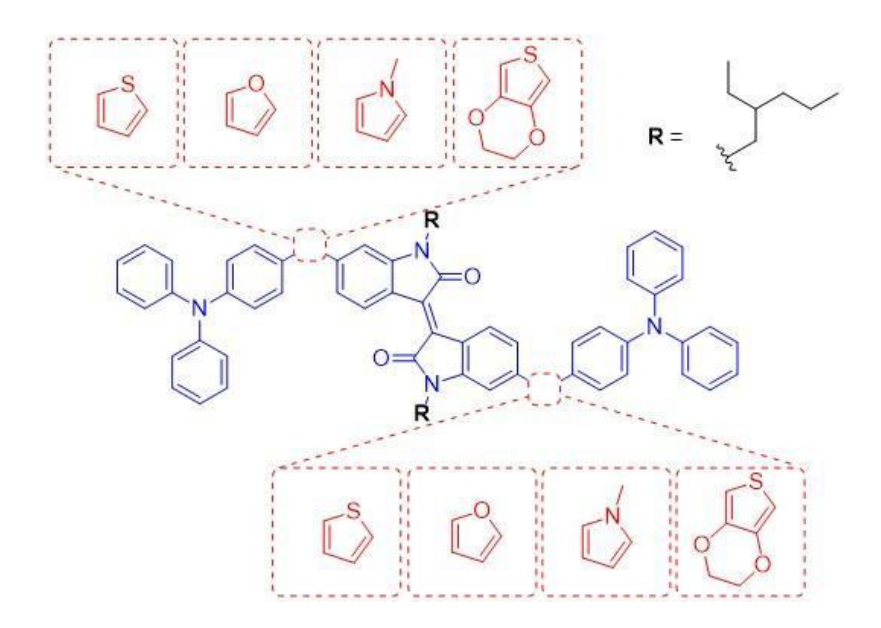


**Figure 1.** Molecular scaffold of isoindigo-based fluorophore targets where the heterocycle donor unit is replaced with either 3,4-ethylenedioxythiophene (**EDOT**), furan (**FURAN**), thiophene (**THIO**), or 1-methyl-1H-pyrrole (**MePyr**).

In this work, we designed four isoindigo based small molecular fluorophores, II-X-TPA (Figure 1). Isoindigo is a natural pigment and has emerged as a promising acceptor scaffold. It has excellent properties such as its highly electron-deficient nature and exceptional solubility after alkylation of the amide nitrogen.30–33 The ideal planar  $\pi$ -conjugated structure of this acceptor core is promoted by the E configuration of the carbon-carbon double bond and is conjugated with two aromatic indole heterocycles.34,35 3,4-Ethylenedioxythiophene (EDOT) is widely used as an exceptional donor possessing a less delocalized lowest unoccupied molecular orbital (LUMO) and is reported to distort molecular backbones and reduce intermolecular/intramolecular interactions while being able to tune the electrostatic potential distribution of the molecule.36–38 Thiophene (THIO), furan (FURAN) and 1-methyl-1H-pyrrole (MePyr) are often used to optimize and investigate the geometry, energetics, and the frontier molecular orbitals of a molecular dye. We have incorporated

these heterocycles as a means to establish the effect of the ring heteroatom on optical properties of the molecular fluorophore. Moreover, it is known that the heteroatom effect is responsible for an additional influence in the properties of the fluorophores in solution such as their reactivity, conformational preference, and their reaction kinetics by redistribution of electron density .46,47 We finalized the molecular design by adding triphenylamine (TPA) as shielding units to the conjugated backbone of the molecular fluorophore and offers additional functionalization at 4,4′-position. The unit assists in preventing unfavorable aggregation and acts as a secondary donor .48—51 In this manuscript, we articulated the experimental and theoretical studies of the II-X-TPA series. This is the first detailed report of photophysical properties and computational studies on the effect of four different heterocyclic donor unit on the isoindigo acceptor. This combined study provides justification for the future project to start with calculations, verified here to be reliable, to select the best candidates for experimental evaluations. Collectively, the design and comparative analysis of these fluorophores present a simple yet promising molecular scaffold for the development of advanced FI agents.

#### **EXPERIMENTAL SECTION**

**Materials and Synthesis:** Reagents and solvents were purchased from commercial sources and used without further purification unless otherwise specified. Anhydrous solvents were obtained with a Glass Contour (Irvine, CA, USA) solvent purification system. Thin-layer chromatography was performed on SiO2-60 F254 aluminum plates with visualization by ultraviolet (UV) light. Flash column chromatography was performed using Purasil SiO2-60, 230–400 mesh from Whatman. The synthesis was derived and modified from previously published works (REF). In

brief, the II-Furan, II-MePyr, and II-Thio derivatives were synthesized using standard Stille conditions. The II-EDOT derivative was synthesized using a C-H activation technique. The II-FURAN-TPA, II-MePyr-TPA, II-THIO-TPA, and II-EDOT-TPA derivatives were synthesized using standard Suzuki conditions. Additional details regarding synthesis and characterization of II-X-TPA derivatives can be found in the supporting information (SI).

**Instrumentation:** Nuclear magnetic resonance (NMR) spectra were recorded on a Bruker (Milton, ON, Canada) 400 MHz spectrometer with the appropriate deuterated solvents. The absorption measurements were done on a Varian Cary-500 spectrometer (Dorval, QC, Canada) in dichloromethane (DCM) while the fluorescence studies were performed on an Edinburgh Instruments FLS-920 fluorimeter with NSG Precision Cells (Farmingdale, NY, USA) cuvettes. Fluorescence quantum yields were measured with samples of low sample concentration (10<sup>-5</sup> M) in DCM and excited close to their maximum absorption. The spectroscopic energy gap (E<sup>opt</sup><sub>g</sub>) was calculated from the onset of absorbance. 72

Fluorescence lifetimes were obtained using the 650 nm output of an LDH series 650P pulsed diode laser as the excitation source (200 microwatts) and a PicoQuant PDM series single photon avalanche diode (time resolution approx. 50 ps) as the detector with a Nikon Eclipse TE2000-U microscope. A TimeHarp 260 time-correlated single photon counter (25 ps resolution) was used to analyze the photons as reported previously [cite 10.1002/chem.201800030]. Lifetimes were acquired in DCM at concentrations of approximately 10<sup>-5</sup> M. The total instrument response function of the setup was determined to be approximately 200 ps.

To calculate the relative quantum yield ( $\Phi$ ) of the samples in solution, the individual samples were excited using a Xenon lamp at the following wavelengths using a Horiba QuantaMaster 8075-

21 Spectrofluorometer: **II-MePyr-TPA** at 610 nm, **II-THIO-TPA** at 605 nm, **II-FURAN-TPA** at 620 nm, and **II-EDOT-TPA** at 640 nm. Emission was measured out to 900 nm using a silicon-based photomultiplier tube detector. Solutions having concentrations of approximately 10<sup>-5</sup> M were placed in quartz cuvettes and capped to reduce the effects of solvent evaporation while under study.

**Computational Methods:** To theoretically explore the geometric and electronic structures of **II-X-TPA** derivatives, density functional theory (DFT) and time-dependent density functional theory (TD-DFT) were employed. Ground state (S<sub>0</sub>) geometry and frequency calculations were performed at DFT/B3LYP/6-311G(d,p) level of theory. To confirm the experimental absorption profile TD-DFT calculations were carried out at OT- $\omega$ B97XD/6-311G(d,p) [OT=optimally tuned]52,53 level of theory54 by considering 10 lowest-lying singlet excited states. In our case, the tuned value of ω is 0.06 Bohr. B3LYP/6-311G(2d,p) level was employed to estimate the frontier orbitals and their energy gap in the **II-X-TPA** derivatives. Full TD-DFT optimizations of the first excited state (S<sub>1</sub>) were performed by OT- $\omega$ B97XD/6-311G(d,p)//OT- $\omega$ B97XD/6-311G(d,p) level of theory and the optimized geometry was used to simulate emission spectra of S<sub>1</sub> state. All calculations were carried out using Gaussian 09 package.[REFERENCE]

#### **RESULTS**

**Design and Synthesis:** The four **II-X-TPA** derivatives were designed to garner an understanding of the effects that different donor heterocycles would have on the optical properties of the resulting derivatives. Donor heterocycles, **THIO**, **FURAN**, **EDOT**, and **MePyr** were all chosen due to their wide use in high-performing optical materials. Thiophene and furan have been studied extensively, each having properties that justify their use in such materials. Incorporating thiophene

allows us to take advantage of the increased aromaticity associated with the heterocycle which can affect the HOMO-LUMO gap of the resulting **II-THIO-TPA** derivative. Furans are known to show increased solubility in polar solvents due to its large dipole moment while being highly fluorescent due to the lack of a heavy atom. 78 Such characteristics are evident in the **II-FURAN-TPA** derivative (vide infra). EDOT is an exceptional heterocyclic donor, with properties that are shown to increase solubility while also possessing enhanced donating ability due to the ether linkage attached to the aromatic ring. 79,77 MePyr was chosen due to its enhanced electron density, ability to act as a donor and to monitor the substituted heteroatoms effect. The TPA flanking unit was chosen to act as an auxiliary donor unit as the TPA moiety provides an increase in the amount of  $\pi$ -electrons while affording a position for further functionalization.82 Furthermore, the propeller-like non-planar twisted structure of TPA gives the target molecules a significant degree of distortion to protect from unfavorable intermolecular interactions(83,84) which commonly influence photophysical properties.80

**Scheme 1. i.** HCl, AcOH, 24h reflux; **ii.** K<sub>2</sub>CO<sub>3</sub>, DMF, 20 h 100 °C; **iii.** Pd(PPh<sub>3</sub>)<sub>4</sub>, toluene (Tol), reflux 24 h; **iv.** NBS, CHCl<sub>3</sub>, under dark, rt 4 h; **v.** aq.Cs<sub>2</sub>CO<sub>3</sub>, Pd(PPh<sub>3</sub>)<sub>4</sub>, Tol:EtOH(1:1), 24 h 100 °C.

Scheme 2. vi. K<sub>2</sub>CO<sub>3</sub>, PdCl<sub>2</sub>, DMAc, 10 min, 1-adamantane carboxylic acid, 10 min, EDOT, 120 °C, 2 hr h; vii. NBS, CHCl<sub>3</sub>, under dark, RT, 4 h; vii. aq.Cs<sub>2</sub>CO<sub>3</sub>, Pd(PPh<sub>3</sub>)<sub>4</sub>, Tol:EtOH(1:1), 24 h 100 °C.

Synthesis of the isoindigo derivatives were performed using Stille coupling conditions for the II-THIO, II-FURAN, and II-MePyr derivatives while a C-H activation technique afforded the II-EDOT as shown in Scheme 1 and Scheme 2. The synthetic details for the II-THIO73 and II-EDOT74 derivatives were obtained and revised from literature while the II-FURAN and II-MePyr derivatives were synthesized using standard Stille conditions. The intermediates (II-THIO, II-FURAN, and II-MePyr) obtained via Stille coupling all were obtained in moderate yields; 70%, 98%, and 75%, respectively. The C-H activation method that provides the II-EDOT intermediate gives varying yields (24-50%) due to the conditions also leading to the formation of an II-EDOT homopolymer. The resulting derivatives were then brominated using NBS in anhydrous CHCl<sub>3</sub>. The TPA functionalized derivatives, II-X-TPA, were then afforded using standard Suzuki conditions. The subsequent Suzuki coupling reactions to obtain the final targets

were all moderate to low yielding, with yields ranging from 34 to 64%. Optimization of the Suzuki conditions was not performed in order to attempt to increase the yields. Each of the final targets were blackish-blue in color in the solid state and a dark blue color in solution, which is indicative of the highly conjugated properties that the fluorophores possess. Full synthetic details and <sup>1</sup>H NMR spectra (S1-S14) can be found in the SI.

**Table 1.** <sup>a</sup>Electrochemical, spectroscopic and <sup>b</sup>DFT computed parameters for the **II-X-TPA** derivatives.

II-X-TPA Derivatives	<i>НОМО<sup>а</sup></i> (eV)	LUMO <sup>a</sup> (eV)	$E_g^{elec}$ (eV)	$\lambda_{onset} \ (nm)$	$E_g^{opt}$ (eV)	HOMO <sup>b</sup> (eV)	LUMO <sup>b</sup> (eV)	$E_{gap}^{HL}^{b}$ (eV)
II-EDOT-TPA	-5.55	-3.54	2.01	798	1.94	-4.83	-2.81	2.02
II-THIO-TPA	-5.60	-3.63	1.97	752	2.05	-5.08	-2.98	2.10
II-FURAN-TPA	-5.58	-3.59	1.99	776	1.99	-4.93	-2.93	2.00
II-MePyr-TPA	-5.56	-3.61	1.95	781	2.03	-4.93	-2.87	2.06

To estimate the energetics of frontier molecular orbitals (FMOs) of II-X-TPA derivatives and their gap B3LYP/6-311+G(2d,p)//B3LYP/6-311G(d,p) level of theory employed. DFT computed HOMO-LUMO gap ( $E_{\rm gap}^{\rm HL}$ ) of the studied II-X-TPA derivatives lies between 2.0 to 2.1 eV where II-FURAN-TPA (2.0 eV) has the lowest and II-THIO-TPA (2.1 eV) has the highest energy gap and all the energetics are summarized in Table 1. The optical HOMO-LUMO gaps ( $E_{\rm g}^{\rm opt}$ ) obtained using spectroscopic analysis is in good agreement with the values obtained computationally with all values falling between 1.94 eV to 2.05 eV. II-EDOT-TPA (1.94 eV) has the smallest  $E_{\rm g}^{\rm opt}$  with the values increasing in the order of II-FURAN-TPA (1.99 eV), II-MePyr-TPA (2.03 eV) and II-THIO-TPA (2.05 eV), respectively. A variation between the  $E_{\rm gap}^{\rm HL}$  and  $E_{\rm gap}^{\rm opt}$  values is that II-

FURAN-TPA is computed to have the lowest HOMO-LUMO gap, whereas experimentally II-EDOT-TPA has the lowest HOMO-LUMO gap. This deviation can be caused by the solvent effect which is not included in DFT calculations. The electrochemically obtained HOMO-LUMO gaps  $(E_g^{\text{elec}})$  lie between 1.95 eV to 2.01 eV. The values do not follow the same trend as the  $E_g^{\text{opt}}$ , however, with **II-MePvr-TPA** having the lowest value (1.95 eV) followed by **II-THIO-TPA** (1.97 eV), II-FURAN-TPA (1.99 eV), and II-EDOT-TPA (2.01 eV). This difference can be rationalized by the solvent effects on the oxidized/reduced species in solution which are distinct with respect to the solvent effects mentioned above. Furthermore, Figure 2 shows the molecular orbitals of II-EDOT-TPA, II-MePyr-TPA, II-FURAN-TPA, and II-THIO-TPA. The computed HOMO energies trend agrees with the electrochemical data but the LUMO energies do not quite align with the trend. This difference is not surprising since the vacant orbitals are generally more difficult to describe theoretically than the occupied ones 55. The HOMO and LUMO energy levels along with  $E_{\rm gap}^{\rm HL}$  and frontier molecular orbitals isoelectronic density distribution are depicted in Figure 2 where the HOMOs of all the targets reveal that the electrons are delocalized throughout the molecule. In contrast, the LUMOs are concentrated around the isoindigo acceptor. Interestingly all the HOMO energies are lower than those of **II-EDOT-TPA**, and **II-THIO-TPA** has the lowest HOMO energy which implies the **THIO** unit stabilizes or lowers the energy of the HOMO of **II**-THIO-TPA.

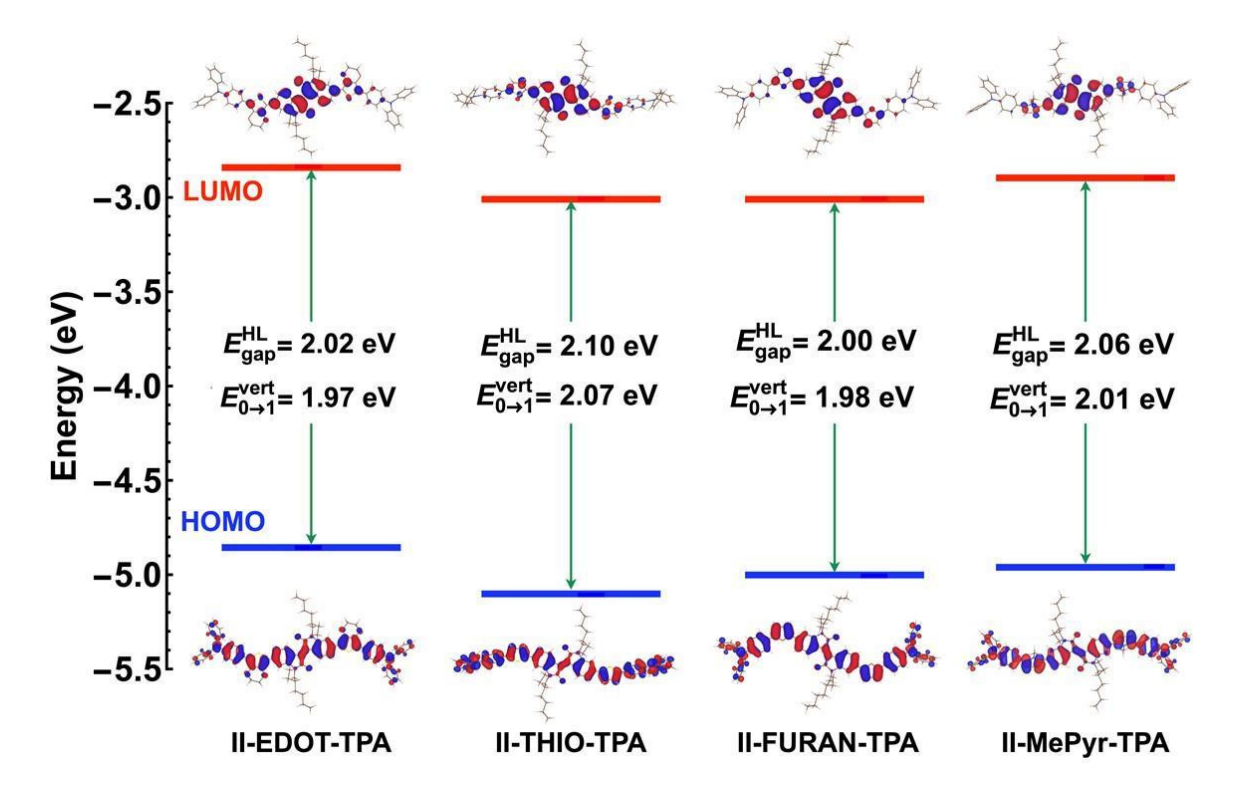


**Figure 2.** Ground state HOMO-LUMO energy gaps  $(E_{gap}^{HL})$ , vertical excitation energy  $(E_{0\rightarrow 1}^{vert})$  along with frontier molecular orbitals density map (isovalue 0.02 au) of the **II-X-TPA** derivatives at the B3LYP/6-311+G(2d,p)// B3LYP/6-311G(d,p) level of theory in the gas phase.

**Spectroscopic Analyses:** With the targets in hand, supported by computational analysis, the absorption and emission studies were undertaken to evaluate the optical properties of the fluorophore dyes. UV-Vis-NIR absorbance spectroscopy was performed and summarized in Table 2, solutions ( $6x10^{-5}$  M in DCM) of each fluorophore (**II-X-TPA**) possess absorption profiles with  $\lambda_{max}^{abs} = 606-640$  nm and  $\lambda_{onset}^{abs} = 752-798$  nm. Figure 3 depicts the absorption profiles of the compounds along with simulated spectra. The broad bands at longer wavelengths arise from  $\pi$ - $\pi$ \* electronic transitions of the conjugated systems and correspond to a transition from the ground singlet state to the lowest excited singlet state of each molecule. The absorption maxima show a

gradual bathochromic shift when changing the donor unit in the order of **II-THIO-TPA** (606 nm), **II-MePyr-TPA** (611 nm), and **II-FURAN-TPA** (622 nm).

**Table 2.** Experimental and theoretical spectroscopic data of the II-X-TPA derivatives including maximum experimental absorption ( $\lambda_{max}^{abs}$ ) and emission ( $\lambda_{max}^{emi}$ ) wavelength in nm, Stokes shift in dichloromethane (DCM) along with molar extinction coefficient (ε). Theoretical absorption ( $\lambda_{max}^{abs}$ ) and emission ( $\lambda_{max}^{emi}$ ) wavelength in nm, absorption ( $E_{abs}$ ) and emission ( $E_{emi}$ ) energy in eV, Stokes shift and oscillator strength (f) of ground ( $S_0$ ) and first excited state ( $S_1$ ). Theoretical values obtained with the use of OT-ωB97XD/6-311G(d,p) level of theory in gas phase.

	Experimental				Theoretical			
II-X-TPA Derivatives	$\lambda_{max}^{abs}$ $(nm)$	$\lambda_{max}^{emi}$ (nm)	Stokes Shift nm (eV)	ε (×10 <sup>4</sup> M <sup>-1</sup> cm <sup>-1</sup> )	$\lambda_{max}^{abs} (E_{abs})$ nm (eV)	$\lambda_{max}^{emi} (E_{emi})$ nm (eV)	Stokes Shift nm (eV)	$f \\ S_0(S_1)$
II-EDOT-TPA	640	805	165 (0.40)	4.3	628 (1.98)	780 (1.59)	152 (0.39)	1.77 (1.43)
II-THIO-TPA	606	771	165 (0.44)	3.4	599 (2.07)	773 (1.60)	173 (0.47)	1.58 (1.41)
II-FURAN-TPA	622	800	178 (0.44)	4.2	627 (1.98)	783 (1.58)	156 (0.40)	1.57 (1.27)
II- MePyr-TPA	611	764	153 (0.41)	3.8	616 (2.01)	773 (1.60)	157 (0.41)	1.40 (1.23)

The experimental molar extinction coefficient ( $\varepsilon$ ) at  $\lambda_{max}$  for the **II-EDOT-TPA**, **II-THIO-TPA**, **III-FURAN-TPA**, and **II-MePyr-TPA** derivatives are 4.3, 3.4, 4.2, and 3.8 ×10<sup>4</sup> M<sup>-1</sup> cm<sup>1</sup> where the theoretical molar extinction coefficients at  $\lambda_{max}$  are computed as 7.3, 6.6, 6.4, and 5.7 ×10<sup>4</sup> M<sup>-1</sup> cm<sup>1</sup> respectively. Moreover, the computed oscillator strengths (f) (Table 2) along with the molar extinction coefficient data confirms that the **II-EDOT-TPA** is capable of harvesting more of the radiation compared to the other derivatives. However, the experimental quantum yields ( $\Phi$ ) for the **II-MePyr-TPA**, **II-EDOT-TPA**, **II-FURAN-TPA**, and **II-THIO-TPA**, derivatives are measured to be 0.012, 0.017, 0.031, and 0.041 % respectively, thus conflicting the interest of **II-EDOT-TPA** by leading the accumulated energy to be released through other pathways than the

desired fluorescence. The excited state lifetimes for **II-MePyr-TPA**, **II-EDOT-TPA**, **II-FURAN-TPA**, and **II-THIO-TPA** derivatives are measured in 6×10<sup>-5</sup> M DCM and were determined to be shorter than 200 ps, the instrument response function of our current setup.

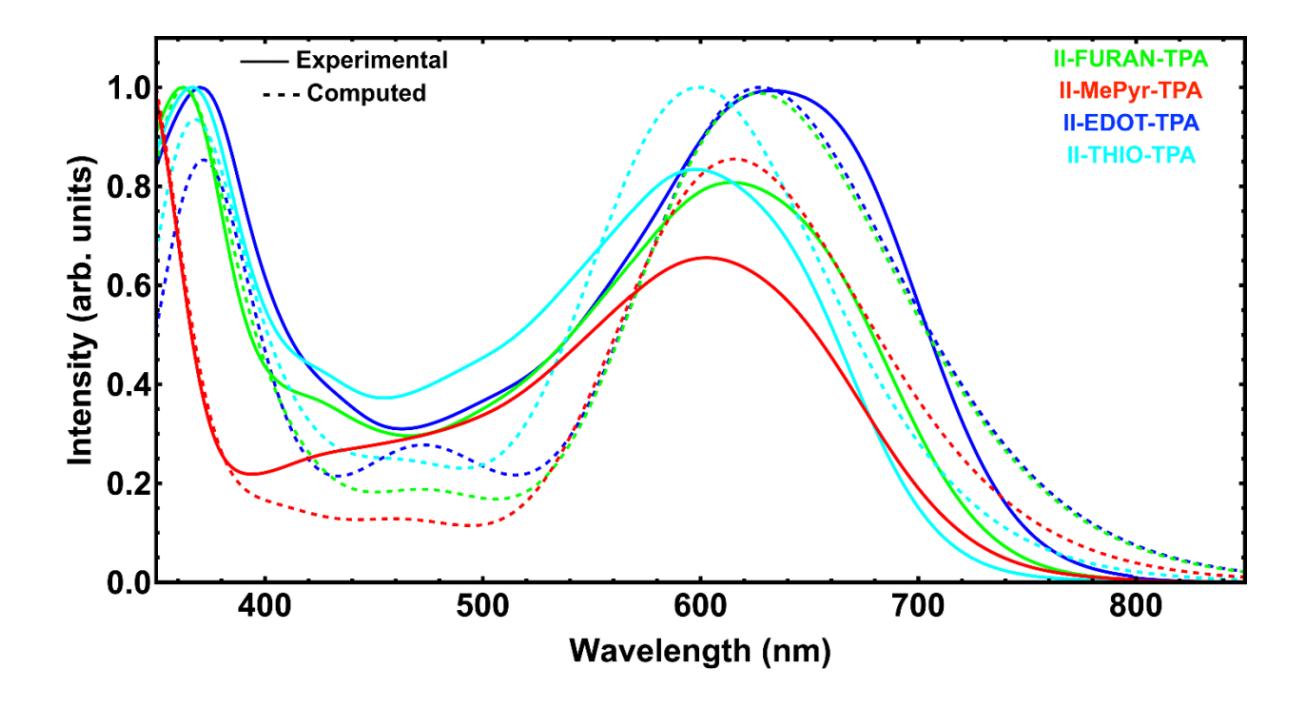


**Figure 3**. Absorption spectra in DCM (solid line) and simulated in gas phase (dashed line) at the  $OT-\omega B97XD/6-311G(d,p)//B3LYP/6-311G(d,p)$  level of theory. To match the broadening of simulated spectra with experimental spectra half width half maxima set at 0.22 eV.

The experimental and computational results obtained for the absorbance are in agreement and can also be correlated to the corresponding maximum emission values. Experimental emission profiles and computed simulated emission spectra are depicted in Figure 4 and the summary of these results is tabulated in Table 2. The effects of the target framework and donor are more pronounced in the fluorescence data. Well-defined single peaks are observed in DCM. Each fluorophore possesses

emission profiles with  $\lambda_{max}^{ems} = 764-805$  nm. The highest emission maximum is observed for II-EDOT-TPA (805 nm) and shows a gradual hypsochromic shift with the change of the EDOT donor unit in the order of FURAN, THIO, and MePyr. There is a noticeable increase with regards to a broadening in the emission peak maxima in the order of II-EDOT-TPA, II-FURAN-TPA, II-THIO-TPA, and II-MePyr-TPA. Similarly, a decrease in the optical energy gap ( $E_g^{opt}$ ) can be seen in the same order. These two trends are evident in the data contained in Table 2 and illustrated in Figure 4.

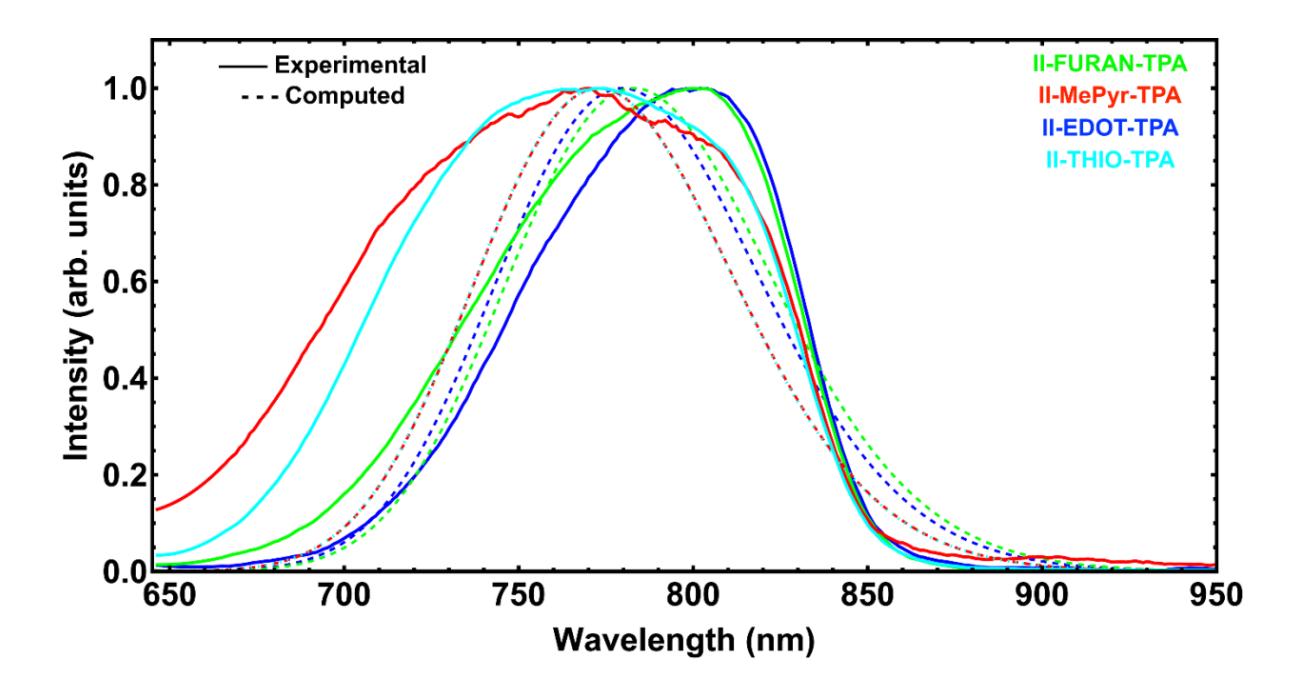
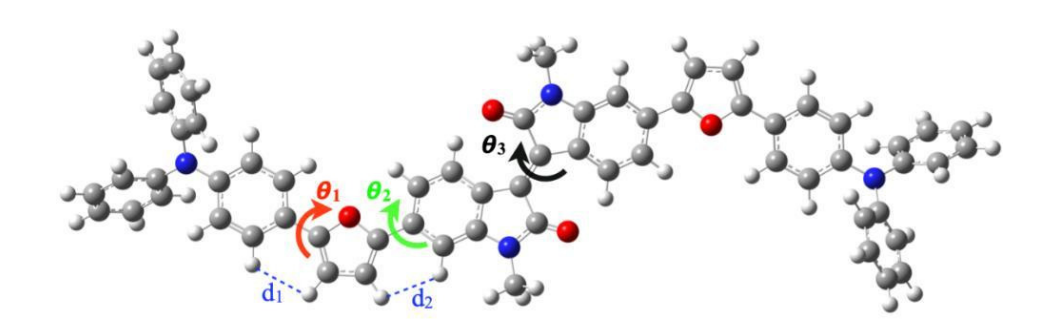


**Figure 4**. Emission spectra of the final target molecules. Dash line indicates the theoretically calculated spectra whereas solid line indicates the experimental emission spectra in DCM. To match the broadening of simulated spectra with experimental spectra half width half maxima set at 0.09 eV.

Table 3. DFT/TDDFT computed different dihedral angle (0), dipole moment (Debye) of ground state ( $\mu$  g) and excited state ( $\mu$  g) optimized geometry of **II-X-TPA** derivatives in gas phase with the use of TD-OT- $\omega$ B97XD/6-311G(d,p)//B3LYP/6-311G(d,p) level of theory.



EH-II Derivatives	$egin{aligned} oldsymbol{ heta_1} \ oldsymbol{ heta_0} \ oldsymbol{ heta_0} \ oldsymbol{ heta_1} \end{aligned}$	$oldsymbol{ heta_2} \left( egin{smallmatrix} \circ \ & \ & \ & \ & \ & \ & \ & \ & \ & \$	$oldsymbol{ heta_3} \left(  ight.  ight) \  ext{S}_0 \left   ext{S}_1  ight.$	μ <sub>S0</sub>   μ <sub>S1</sub> (Debye)	$d_{I}$ (Å) $S_{0}   S_{1}$	$egin{aligned} d_2( ext{Å}) \ & \mathbf{S_0} \mid \mathbf{S_1} \end{aligned}$
EDOT-TPA	27.31   22.73	3.36   12.90	14.26   28.27	0.75   0.64	2.43   2.36*	2.21   2.26*
THIO-TPA	29.82   20.72	26.52   13.41	16.18   28.67	0.41   1.10	2.43   2.31	2.38   2.20
<b>FURAN-TPA</b>	6.07   2.14	4.26   3.64	13.92   28.31	0.87   2.64	2.41   2.42	2.38   2.39
MePyr-TPA	46.76   36.90	39.69   37.22	14.05   29.25	3.41   1.92	2.83   2.59	2.61   2.54
Isoindigo			10.88	0.36		

H—O bond

The dihedral angles and important bond lengths along with the dipole moments are tabulated in Table 3. The computed ground state dipole moment is higher than those of the S<sub>1</sub> for **EDOT** and MePyr derivatives while THIO and FURAN show the opposite trend. Isoindigo is a nonplanar molecule containing E-stilbene units belonging to the C<sub>2</sub> point group. Substitution in 6,6'- and 5,5'position of benzene ring attributes to its distinguished structural patterns and electronic properties. 56 Stalder et al. also found that the type of substituent does not affect the LUMO level while it destabilizes the HOMO energy level. We observed that the inter-ring dihedral angle of isoindigo is  $10.88^{\circ}$  which is not perturbed more than around  $\pm$  1° with the substitution in the ground state geometry. Perpète et al. also reported that the inter-ring dihedral angle of isoindigo is close to 15° and is mostly unchanged by substitution, except for the inclusion of a methyl group at the nitrogen of the pyrrole (**MePyr**), which gives a stronger steric hindrance, and increases the twist to about 23°.57 In our DFT study, we found that that the HOMO - LUMO energy is aligned with the reported value using the same level of theory. The transition from  $S_0 \rightarrow S_1$  occurred at 495.17 nm with the contribution HOMO $\rightarrow$ LUMO (93%) and HOMO-2 $\rightarrow$ LUMO ( $\sim$ 5%) with an oscillator strength of 0.1078.

### **DISCUSSION**

The goal of this work was to identify a versatile molecular fluorophore scaffold, which operates in the NIR region. For this purpose, a strong acceptor (isoindigo) was functionalized with a donor unit to lower the HOMO-LUMO energy gap. Once isoindigo was fitted with a series of heterocyclic donors, small molecule fluorophores II-X-TPA were afforded with remarkable diverse optical properties. The experimental analysis of the optical properties correlates well with the results obtained from the computational analysis. It is noted that the absorbance and emission profiles for all four donor units have comparable values with II-EDOT-TPA having the most redshifted absorbance (640 nm) and emission (805 nm) peak maxima followed by II-FURAN-TPA, II-THIO-TPA, and II-MePyr-TPA in that order. It should be noted that the LUMO is being contributed by the isoindigo acceptor, whereas the HOMO is more controlled by the heterocycle donor. Here, EDOT is an efficient electron transferring agent and an electron rich unit (77), which raise the HOMO. Therefore, II-EDOT-TPA has the lowest HOMO-LUMO energy gap hence, the longer wavelength absorption and emission maxima. The other heteroatomic donors possess similar qualities that make their optical properties distinguishable from each other, but for the most

part, do not rival the experimental properties of **II-EDOT-TPA** due to several reasons all of which surround the donor heterocycle being employed.

Properties of heteroatomic compounds are dominated by the changes in the  $\pi$ -electron charge distribution. 59 The heterocycles, FURAN, THIO, and MePyr exhibit similar energy levels and a comparable degree of aromaticity. 59 Heterocycle, MePyr has a higher degree of aromaticity whereas FURAN has the lowest. This is consistent with the degree of delocalization of the  $\pi$ electrons. An increase in the degree of aromaticity and the delocalization of  $\pi$ -electrons will negatively correlate with HOMO-LUMO energy gap (Table 1).60 The spectroscopic analysis indicates II-EDOT-TPA with lowest  $E_g^{opt}$  (1.94 ev) is phenomenal compared to the other II-X-**TPA** series (discussion below). Unlike fused aromatic compounds, α-linked conjugated heterocycles adopt a non-aromatic quinoidal structure at the expense of their aromatic stabilization.61–65 Theoretical calculations suggest that II-EDOT-TPA has a nearly coplanar conformation between the acceptor and the EDOT ( $\theta_2$ = 3.36) when the molecule is in the ground state. This coplanarity provides an extension to delocalization and is due to pseudo-hydrogen bonding between the oxygen on the EDOT ether moiety and the hydrogen on the acceptor phenyl moiety, having a bond distance of 2.21 Å. However, the TPA hydrogen is much further away, weakening the interaction, which allows for some distortion from the backbone. The heterocycle FURAN is the smallest donor unit hence II-FURAN-TPA is planar at the ground state. FURAN is the least aromatic heterocycle, allowing it to be more susceptible to achieve the quinoidal resonance form by delocalization of the electron density through conjugated carbons instead of oxygen and has the planar geometry in the excited state. 66–68 With **THIO** being larger in size, an increase in repulsive interactions with the acceptor and TPA unit results in a non-coplanar geometry in the ground state (29.82°) when compared to the excited state (20.72°).68,69

Unlike the **FURAN** heterocycle, **THIO** shows delocalization of electron density through the heteroatom, which results in a more twisted excited state geometry in the **II-X-TPA** derivative.66–68,70 Moreover, **II-MePyr-TPA** has a bulky methyl unit at the nitrogen atom of **MePyr**, which is unfavorable for its planarity at the ground state as well as the excited state.68,71 The large dihedral angle between the **THIO** (S<sub>0</sub>|S<sub>1</sub>: 26.52 ° |13.41 °) and **MePyr** (S<sub>0</sub>|S<sub>1</sub>: 39.69 ° |37.22 °) units and the six-member ring of the isoindigo acceptor suggests an increase in steric hindrance between the donor and acceptor moieties.58

To understand the electronic transition and charge transfer phenomena in the isoindigo derivatives, the UV-vis-NIR absorption spectra, and excitation related FMOs were analyzed. The optimized structures of the compounds are documented in the SI. In Figure 1, the DFT computed FMOs are depicted graphically and all the  $S_0 \rightarrow S_n$  transition data (oscillator strength > 0.1) are tabulated in Table 2 and Table S1. TD-DFT simulated UV-Vis-NIR absorption spectra are presented in Figure 3. The salient features (shape and the location of peaks) of the TD-DFT simulated spectra agree with the experimental observations. The LUMOs are primarily localized on the isoindigo core and partially extend onto the heterocycles. Although all the  $S_0 \rightarrow S_1$  transitions mainly involve the HOMO \rightarrow LUMO (>90\%), we also observe that an electron density redistribution from the substituents to the isoindigo core involving HOMO−2 → LUMO, with small contributions ~7-8% except II-THIO-TPA (~16%). These observations suggest ICT between the substituents and the isoindigo core occurring by an  $S_0 \rightarrow S_1$  transition. In most cases, higher energy transition, specifically  $S_0 \rightarrow S_9$ , with significant oscillator strength compare to the lowest energy transition except in II-MePyr-TPA. In II-MePyr-TPA, transition  $(S_0 \rightarrow S_8)$ centered at 3.61 eV presents large oscillator strength (1.57) contrary to that with the lowest energy transition (1.40), are highly mixed, with contributions coming from several one-electron excitations. To confirm the ICT band, we perform natural transition orbital (NTO) analysis. NTO analysis revealed that the higher energy (3.61 eV) transition not predominately involves HOMO 

LUMO transition and highly localized whereas lowest energy transition predominately HOMO-LUMO (Figure S23) with delocalized distribution. Based on the orbital shapes and delocalization of electron density depicted in Figure 2 (Figure S15-S18), all the low energy transitions where the electron densities shift from donor units to the isoindigo core unit are  $\pi \rightarrow \pi^*$ excitations. However, for transitions centered at higher energies, electron density distributions are more localized. The oscillator strength  $S_0 \rightarrow S_1$  transition for the studied small molecules ranges from 1.40 to 1.77 where **II-EDOT-TPA** holds the maximum value, suggesting a strong electronic coupling between the charge-transfer states (CT) which confirms the higher ICT. Transitions centered at higher energies are primarily related to HOMO-6→LUMO, HOMO-4→LUMO, HOMO-2→LUMO, HOMO→LUMO+2 and HOMO→LUMO. These types of observations suggest that excitation of the studied compounds at higher energy stems from lower HOMO levels. It should be noted that in all studied **II-X-TPA** derivatives, the lowest singlet excitation is the one with the largest transition probability (f) and originated from the HOMO-LUMO excitation. Moreover, in the case of emission, the most dominant transition for  $S_0 \leftarrow S_1$  is HOMO $\leftarrow$ LUMO.

To reveal the origin of the Stokes shift, predicted ground and excited state geometries were analyzed. Front and side views of the ground state (S<sub>0</sub>) and first excited state (S<sub>1</sub>) optimized geometries are depicted in Figure S19 -S22. In the ground state, **H-EDOT-TPA** has a planar geometry with a dipole moment of 0.75 Debye compared to the first excited state in which the twist angle,  $\theta_2$ , is perturbed (3.36° to 12.90°) from the conjugated backbone, which decreases the dipole moment to 0.64 Debye. It is notable to mention that in the excited state, the EDOT unit is perturbed from the **H-EDOT-TPA** plane. Compared to **H-EDOT-TPA**, the dipole moment ( $\mu_{S0}$ )

of II-THIO-TPA is lower which indicates that the degree of planarity is decreased. The excited state geometry of II-THIO-TPA is more planar than the ground state, where  $\theta_2$  decreased from  $26.52^{\circ}$  to  $13.410^{\circ}$  and achieved a higher dipole moment. FURAN is more planar in the excited state than its ground state geometry and the dipole moment increased from 0.87 to 2.64 Debye which is presumed to be a consequence of the mesomeric effect. However, II-THIO-TPA shows a significant increase in computed Stokes shift which arises from the steric repulsion between the hydrogen atoms of the thiophene ring and the hydrogen atoms of the TPA and isoindigo benzene units. The trend obtained in TD-DFT for emission spectra does not follow experimental findings due to the simplified model applied that does not include solvation in the excited state. In all the cases, the bond length between TPA and donor, as well as donor and isoindigo units decreased by 0.01 Å in  $S_1$  geometry compare to  $S_0$ , except II-MePyr-TPA where the length remains same.

The observed experimental trends are consistent with those obtained from theoretical calculations summarized in Table 2 and lower excited states related data (Table S1). Each fluorophore possesses theoretical absorption profiles with  $\lambda_{max}$ = 599 - 627 nm in which **II-EDOT-TPA** shows the highest absorption maxima (627 nm) and shows a gradual hypsochromic shift when changing the donor unit in the order of **FURAN**, **MePyr**, and **THIO**. This trend enforces the idea that the **EDOT** donor is best suited for the isoindigo acceptor. Regarding the emission characteristics (Figure S23), the calculations underestimate the experimental wavelengths. Even though, the computed absorption maximum trend is in good agreement with the experimental observations, the oscillator strengths (f) do not completely correspond with the experimental molar extinction coefficients ( $\epsilon$ ) as we did not include the solvent effect in DFT calculation framework (Table 2). It should be noted that theoretical calculations were performed for an isolated molecules. However, under experimental conditions, the interaction between

solvent molecules and the **II-X-TPA** derivatives with strong charge separation may significantly affect the energy levels and excitation processes.

In a review of the emission profiles, the shape of the emission band varies with the heterocycle as show in Figure 4. II-MePyr-TPA shows the highest broadening and the peaks become sharper in the order of II-THIO-TPA, II-FURAN-TPA, and II-EDOT-TPA. Evidently the heterocycle moieties and the two aromatic indole heterocycle units are deviating from the conjugated backbone when relaxing from  $S_1$  to  $S_0$  and require additional energy for reorganization (Table 3). Usually, the additional energy for the internal rotation is a non-radiative energy loss that occurs at the excited state, leaving limited numbers of photons that are observed as fluorescence, hence the lower  $\Phi$  as well as the excited state lifetimes. Additionally, all of the II-X-TPA fluorophores have  $\Phi$  of <1%, emission lifetimes <200 ps (Figure S24). High  $\varepsilon$  and low  $\Phi$ /emission lifetime could be an indication of heat generation. Comprehensively theoretical calculations qualitatively agree with the experimental observations. Observed structural rearrangement in the excited state geometry sheds light on the significant Stokes shift of II-X-TPA fluorophores. These results suggest that the ICT, bond length and dihedral angle can be controlled by the donor strength in the coplanar D-A-D compounds.

#### **CONCLUSIONS**

In summary, a series of four isoindigo-based NIR active fluorophores were designed, synthesized, and characterized. UV-Vis-NIR absorbance studies show that each of the fluorophores possesses a strong wide absorption peak, which indicates a low energy gap between the HOMO-LUMO orbitals. Absorbance peak maxima showed a bathochromic shift when changing the heterocyclic donor unit from Thiophene, 1-Methyl-1H-pyrrole, Furan to EDOT in that order. The fluorophores

were found to emit in the NIR region with large Stokes shifts (>0.4 eV) due to intramolecular

charge transfer phenomena. Computational studies reveal that the molecular geometry alterations

are attributed to steric hindrance between the heterocyclic donor and the isoindigo core and TPA

unit. In the case of II-EDOT-TPA, hydrogen bonding occurs between the oxygen of the ether

moiety on the EDOT and the hydrogen on the isoindigo core in both the ground state as well as

the first excited state. Importantly, the donor units with heterocycles control the bond length and

dihedral angle between the donor and the isoindigo acceptor which can alter the Stokes shift as

well as redshift the absorbance and emission peak maxima.

ASSOCIATED CONTENT

Supporting Information. Supporting materials contain experimental details regarding synthesis,

spectra, and other supplementary results. This material is available free of charge via the Internet

at http://pubs.acs.org.)

**AUTHOR INFORMATION** 

**Corresponding Author** 

\*dwatkins@olemiss.edu; jerzy@icnanotox.org

**Author Contributions** 

The manuscript was written through the contributions of all authors. All authors have given

approval to the final version of the manuscript.

**Funding Sources** 

NSF OIA-1757220

1

# ACKNOWLEDGMENT

The authors appreciate the financial support of this work from the National Science Foundation under Grant Number NSF OIA-1757220. JKR and JL acknowledge the Mississippi Center for Supercomputing Research (MCSR) for providing state-of-the-art high-performance computing facilities and outstanding services for supporting this research.